

Tunable magnomechanically and optomechanically induced transparency in a cavity opto-magnomechanical system

Ke Di(邸克), Huarong Xia(夏华容), Wenting Diao(刁文婷), Chunxiao Cai(蔡春晓), Wenhai Yang(杨文海), Yulian Qin(秦瑜莲), Ziting Liao(廖子婷), Yucan He(何钰灿), and Jiajia Du(杜佳佳)
Citation: Chin. Phys. B, 2025, 34 (**7**): 074201. DOI: 10.1088/1674-1056/adc18f
http://cpb.iphy.ac.cn; http://iopscience.iop.org/cpb

What follows is a list of articles you may be interested in

Multiple induced transparency in a hybrid driven cavity optomechanical device with a two-level system

Wei Zhang(张伟), Li-Guo Qin(秦立国), Li-Jun Tian(田立君), and Zhong-Yang Wang(王中阳)
Chin. Phys. B, 2021, 30 (**9**): 094203. DOI: 10.1088/1674-1056/abf642

Controlling multiple optomechanically induced transparency in the distant cavity-optomechanical system

Rui-Jie Xiao(肖瑞杰), Gui-Xia Pan(潘桂侠), and Xiao-Ming Xiu(修晓明)
Chin. Phys. B, 2021, 30 (**3**): 034209. DOI: 10.1088/1674-1056/abc7a4

Compound-induced transparency in three-cavity coupled structure

Hao-Ye Qin(秦昊烨), Yi-Heng Yin(尹贻恒), and Ming Ding(丁铭)
Chin. Phys. B, 2020, 29 (**12**): 124208. DOI: 10.1088/1674-1056/abab7e

Polarization-insensitive complementary metamaterial structure based on graphene for independently tuning multiple transparency windows

Hailong Huang(黄海龙), Hui Xia(夏辉), and Hongjian Li(李宏建)
Chin. Phys. B, 2020, 29 (**11**): 114203. DOI: 10.1088/1674-1056/abb307

Control of microwave signals using bichromatic electromechanically induced transparency in multimode circuit electromechanical systems

Cheng Jiang(江成), Yuanshun Cui(崔元顺), Xintian Bian(边心田), Xiaowei Li(李晓薇), Guibin Chen(陈贵宾)
Chin. Phys. B, 2016, 25 (**5**): 054204. DOI: 10.1088/1674-1056/25/5/054204

Tunable magnomechanically and optomechanically induced transparency in a cavity opto-magnomechanical system

Ke Di(邸克)[1,3], Huarong Xia(夏华容)[1], Wenting Diao(刁文婷)[2], Chunxiao Cai(蔡春晓)[2], Wenhai Yang(杨文海)[2], Yulian Qin(秦瑜莲)[1], Ziting Liao(廖子婷)[1], Yucan He(何钰灿)[1], and Jiajia Du(杜佳佳)[1,†]

[1] *Chongqing University of Posts and Telecommunications, Chongqing* 400065, *China*
[2] *Xi'an Branch of China Academy of Space Technology, State Key Laboratory of Millimeter Waves, Xi'an* 710100, *China*
[3] *State Key Laboratory of Quantum Optics and Quantum Optics Devices, Shanxi University, Taiyuan* 030006, *China*

(Received 27 December 2024; revised manuscript received 13 March 2025; accepted manuscript online 18 March 2025)

We demonstrate multiple transparency windows in a cavity opto-magnomechanical system containing a ferromagnetic material yttrium iron garnet (YIG) crystal. The probe output spectrum reveals the simultaneous emergence of three distinct phenomena: magnon-induced transparency (MIT) arising from microwave–magnon coupling; magnomechanically induced transparency (MMIT) through phonon–magnon interaction, and optomechanically induced transparency (OMIT) mediated by optical cavity–photon coupling. Crucially, these transparency features demonstrate dynamic tunability through precise manipulation of the number of interacting modes and coupling strengths. Our study reveals the effects of magnon–microwave and optomechanical coupling on probe results and the role of quantum interference mechanisms in a resonant system. Moreover, the fast-slow light effect can be enhanced and switched by choosing appropriate coupling parameters. Our work has potential applications in multi-band quantum storage and multi-channel photonic information processing devices.

Keywords: cavity opto-magnomechanical system, transparency windows, Fano resonances, fast-slow light

PACS: 42.50.Ct, 42.50.–p, 42.50.Md, 42.50.Nn

DOI: 10.1088/1674-1056/adc18f **CSTR:** 32038.14.CPB.adc18f

1. Introduction

The cavity optomechanics (COM) system serves as a platform for investigating the mechanical and optical mode coupling in an optical cavity mediated by radiation pressure.[1] Modulating the energy levels in the COM system can induce many unique optical effects, such as optomechanically induced transparency (OMIT),[2] optomechanically induced absorption (OMIA),[3] quantum phase transitions,[4] non-reciprocal transport[5] and ground-state cooling.[6] The system has potential applications in quantum memory,[7] measuring charge[8] and optical storage.[9]

Researchers have recently extended related studies to the cavity magnomechanics (CMM) system, which is similar to the COM system.[10] The CMM system is constructed from ferromagnetic materials, including the magnetic insulator yttrium iron garnet (YIG) crystal, which exhibits a low damping rate and a very high spin density.[11] Consequently, it provides a promising foundation for exploring diverse quantum phenomena, including magnomechanically induced transparency (MMIT),[12] magnomechanically induced absorption (MMIA),[13] mechanical cooling,[14] bistability,[15] nonreciprocal magnon blockade[16] and quantum entanglement.[17] The magnon of spin waves in YIG crystal is robust to temperature[18] and magnetically induced transparency (MIT) at room temperature has been demonstrated in the CMM system.[10,19] YIG crystals introduce magnon–phonon interactions through the magnetostrictive effect and generate MMIT, similar to electromagnetically induced transparency (EIT).[20] MMIT results from quantum sideband interference effects triggered by the interaction between magnon and phonon.

Based on the above studies, we find that previous research on transparency windows has typically been limited to the separate investigation of MIT, MMIT, and OMIT, with a primary focus on the COM and CMM systems. Although these studies have adopted different theoretical frameworks and technical approaches, most have not fully revealed the coexistence mechanisms underlying multiple transparency windows. To address this limitation, our study proposes an innovative scheme for simultaneously realizing multiple transparency windows, including MIT, MMIT and OMIT, within a cavity opto-magnomechanical (OMM) system.[21] Specifically, we utilized a YIG crystal with a micro bridge structure as a conduit to connect the microwave and optical cavities effectively. In the cavity-OMM system, the magnon mode couples with the microwave cavity mode through magnetic dipole interaction.[22] The magnetostrictive force couples the magnon mode to the phonon mode,[23] while the phonon mode couples with the optical cavity mode via the radiation pressure effect.[24] By modifying the interaction strengths within the system, we can flexibly control the number, width and depth

†Corresponding author. E-mail: dujj@cqupt.edu.cn

© 2025 Chinese Physical Society and IOP Publishing Ltd. All rights, including for text and data mining, AI training, and similar technologies, are reserved.

of the transparency windows. Additionally, we observe Fano resonance and fast-slow light effects in the output field,[25,26] and dynamically convert between multi-channel fast and slow light phenomena. The Fano resonance arises from quantum interference in the resonant states of different systems and is characterized by sharp and asymmetric resonance spectral lines.[27] Fast-slow light arises from the absorption and dispersion of light waves propagating through a medium, leading to substantial variations in the group velocity of light.[28] By tuning the frequency of the probe field varying within the microwave and optical frequency bands, resonance is achieved separately with the microwave cavity and the optical cavity. Consequently, the coexistence of multiple transparency windows demonstrated in our study has potential applications in the development of multi-band quantum storage and multi-channel photonic information processing devices.[29]

2. Theoretical model

Figure 1(a) illustrates the cavity-OMM system, which includes the microwave cavity mode (a), magnon mode (m), phonon mode (b), and optical cavity mode (c). Two highly reflective mirrors construct the optical cavity and fix the micro bridge YIG crystal to the right cavity mirror.[30] The microwave field is introduced into the system through the cavity port and forms the microwave cavity. The strong red-detuned microwave field and optical field are used to drive the magnon mode and optical cavity mode, respectively.[31] When the magnon mode is excited, the change in magnetization intensity triggers the lattice deformation to generate the phonon mode. The phonon mode is coupled to the optical cavity and the magnon mode via the radiation pressure mechanism and the nonlinear magnetostrictive effect.[21] Simultaneously, the magnon mode couples to the microwave cavity mode through the magnetic dipole effect.[32] Meanwhile, two weak probe fields are used to probe the output response of the two cavity modes separately. The Hamiltonian of the system is expressed as

$$\begin{aligned} H/\hbar =\ & \omega_a a^\dagger a+\omega_b b^\dagger b+\omega_c c^\dagger c+\omega_m m^\dagger m \\ & +g_{ma}(a^\dagger m+am^\dagger)+g_{mb}m^\dagger m(b+b^\dagger) \\ & -g_{bc}c^\dagger c(b+b^\dagger)+\mathrm{i}\varepsilon_{\mathrm{p1}}(a^\dagger \mathrm{e}^{-\mathrm{i}\omega_{\mathrm{p1}}t}-a\mathrm{e}^{\mathrm{i}\omega_{\mathrm{p1}}t}) \\ & +\mathrm{i}\varepsilon_{\mathrm{p2}}(c^\dagger \mathrm{e}^{-\mathrm{i}\omega_{\mathrm{p2}}t}-c\mathrm{e}^{\mathrm{i}\omega_{\mathrm{p2}}t})+H_{\mathrm{dri}}, \end{aligned} \tag{1}$$

where a ($a^\dagger$), m ($m^\dagger$), b ($b^\dagger$), and c ($c^\dagger$) are the annihilation (creation) operators of the microwave cavity mode, magnon mode, phonon mode and optical cavity mode, which satisfy the canonical logarithmic relation $[j,j^\dagger]=1$. ω_j ($j=a,m,b,c$) is the frequency of the four modes. The magnon mode frequency is determined by $\omega_m=\gamma H$, where H is the external bias magnetic field and γ is the gyromagnetic ratio.[33] The fifth, sixth, and seventh terms in Eq. (1), g_{ma} denotes the microwave–magnon coupling strength, while g_{mb} and g_{bc} represent the magnonmechanical and optomechanical coupling strengths. The last term is the driving Hamiltonian, $H_{\mathrm{dri}}=\mathrm{i}\Omega(m^\dagger \mathrm{e}^{-\mathrm{i}\omega_0 t}-m\mathrm{e}^{\mathrm{i}\omega_0 t})+\mathrm{i}E(c^\dagger \mathrm{e}^{-\mathrm{i}\omega_{\mathrm{L}}t}-c\mathrm{e}^{\mathrm{i}\omega_{\mathrm{L}}t})$, where the Rabi frequency $\Omega=(\sqrt{5}/4)\gamma\sqrt{N}B_0$ denotes the coupling strength between the magnon mode and the microwave drive field, with amplitude B_0 and frequency ω_0. $N=\rho V$ is the total number of spins in the YIG crystal.[33] $E=\sqrt{2P_{\mathrm{L}}\kappa_c/\hbar\omega_{\mathrm{L}}}$ represents the coupling strength between the optical cavity and the driving laser, where κ_c is the decay rate of the optical cavity, and $P_{\mathrm{L}}(\omega_{\mathrm{L}})$ is the power (frequency) of the laser field with a wavelength of 1550 nm.[34] In addition, ω_{P1} and ω_{P2} are the frequencies of the two weak probe fields acting in the microwave and optical cavities with amplitudes $\varepsilon_{\mathrm{p1}}=\sqrt{2P_1\kappa_a/\hbar\omega_{\mathrm{p1}}}$ and $\varepsilon_{\mathrm{p2}}=\sqrt{2P_2\kappa_c/\hbar\omega_{\mathrm{p2}}}$.

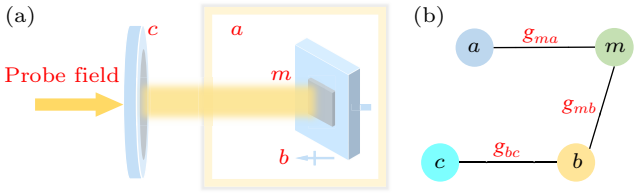


Fig. 1. (a) Sketch of the cavity-OMM system. Specifically, the microwave cavity and magnon modes are coupled through magnetic dipole interaction. The phonon mode is coupled to the magnon mode via dispersive magnetostriction and to the optical cavity via radiation pressure. (b) The equivalent physical model.

In Eq. (1), we neglect the nonlinear term $Km^\dagger m^\dagger mm$ that the strongly driven magnon mode may introduce.[35] To ensure the validity of this approximation, the condition $K|\langle m\rangle|^3\ll\Omega$ must be satisfied,[36] which is always satisfied by the parameters in our system. In the frame rotating at the driving frequencies ω_{L} and ω_0, the modified Hamiltonian is

$$\begin{aligned} H/\hbar =\ & \Delta_a a^\dagger a+\omega_b b^\dagger b+\Delta_c c^\dagger c+\Delta_m m^\dagger m \\ & +g_{ma}(a^\dagger m+am^\dagger)+g_{mb}m^\dagger m(b+b^\dagger) \\ & -g_{bc}c^\dagger c(b+b^\dagger)+\mathrm{i}\Omega(m^\dagger-m) \\ & +\mathrm{i}E(c^\dagger-c)+\mathrm{i}\varepsilon_{\mathrm{p1}}\left(a^\dagger \mathrm{e}^{-\mathrm{i}\delta_1 t}-a\mathrm{e}^{\mathrm{i}\delta_1 t}\right) \\ & +\mathrm{i}\varepsilon_{\mathrm{p2}}\left(c^\dagger \mathrm{e}^{-\mathrm{i}\delta_2 t}-c\mathrm{e}^{\mathrm{i}\delta_2 t}\right), \end{aligned} \tag{2}$$

where the detuning parameters are expressed as $\Delta_a=\omega_a-\omega_0$, $\Delta_m=\omega_m-\omega_0$, $\Delta_c=\omega_c-\omega_{\mathrm{L}}$, $\delta_1=\omega_{\mathrm{p1}}-\omega_0$ and $\delta_2=\omega_{\mathrm{p2}}-\omega_{\mathrm{L}}$. Including the dissipation and input noise of each mode, the quantum dynamics of the system can be described by the following Heisenberg–Langevin equations:

$$\dot{a}=-\mathrm{i}\Delta_a a-\kappa_a a-\mathrm{i}g_{ma}m+\varepsilon_{\mathrm{p1}}\mathrm{e}^{-\mathrm{i}\delta_1 t}+\sqrt{2\kappa_a}a^{\mathrm{in}}(t), \tag{3}$$

$$\begin{aligned} \dot{m}=\ & -\mathrm{i}\Delta_m m-\kappa_m m-\mathrm{i}g_{ma}a-\mathrm{i}g_{mb}m(b+b^\dagger) \\ & +\Omega+\sqrt{2\kappa_m}m^{\mathrm{in}}(t), \end{aligned} \tag{4}$$

$$\begin{aligned} \dot{b}=\ & -\mathrm{i}\omega_b b-\kappa_b b-\mathrm{i}g_{mb}m^\dagger m+\mathrm{i}g_{bc}c^\dagger c \\ & +\sqrt{2\kappa_b}b^{\mathrm{in}}(t), \end{aligned} \tag{5}$$

$$\dot{c} = -\mathrm{i}\Delta_c c - \kappa_c c + \mathrm{i}g_{bc}c(b+b^\dagger) + E + \varepsilon_{\mathrm{p}2}\mathrm{e}^{-\mathrm{i}\delta_2 t} + \sqrt{2\kappa_c}c^{\mathrm{in}}(t), \quad (6)$$

where κ_j and j^{in} $(j = a, m, b, c)$ are the dissipation rates and vacuum input noise operators of the microwave cavity, magnon, phonon, and optical cavity modes. Under the condition of a strong driving field, the magnon mode and the optical mode have a large amplitude $|\langle m_{\mathrm{s}}\rangle|, |\langle c_{\mathrm{s}}\rangle| \gg 1$ in the steady state.[31] Due to beam splitter interactions, the microwave cavity mode can obtain steady-state amplitudes $|\langle a_{\mathrm{s}}\rangle| \gg 1$. Then, we decompose each operator into the sum of a steady-state term and a fluctuation term, i.e., $O = O_{\mathrm{s}} + \delta O$ $(O = a, m, b, c)$.[37] We obtain the steady-state solutions of the dynamic operator as

$$a_{\mathrm{s}} = \frac{-\mathrm{i}g_{ma}m_{\mathrm{s}}}{\mathrm{i}\Delta_a + \kappa_a}, \quad (7)$$

$$m_{\mathrm{s}} = \frac{-\mathrm{i}g_{ma}a_{\mathrm{s}} + \Omega}{\mathrm{i}\widetilde{\Delta}_m + \kappa_m}, \quad (8)$$

$$b_{\mathrm{s}} = \frac{-\mathrm{i}g_{mb}|m_{\mathrm{s}}|^2 + \mathrm{i}g_{bc}|c_{\mathrm{s}}|^2}{\mathrm{i}\omega_b + \kappa_b}, \quad (9)$$

$$c_{\mathrm{s}} = \frac{E}{\mathrm{i}\widetilde{\Delta}_c + \kappa_c}, \quad (10)$$

where the effective detunings are $\tilde{\Delta}_m = \Delta_m + g_{mb}(b_{\mathrm{s}} + b_{\mathrm{s}}^\dagger)$ and $\tilde{\Delta}_c = \Delta_c - g_{bc}(b_{\mathrm{s}} + b_{\mathrm{s}}^\dagger)$. Considering only the first-order sideband effects of the system, the equation of motion for the fluctuation terms is obtained as

$$\delta\dot{a} = -(\mathrm{i}\Delta_a + \kappa_a)\delta a - \mathrm{i}g_{ma}\delta m + \varepsilon_{\mathrm{p}1}\mathrm{e}^{-\mathrm{i}\delta_1 t}, \quad (11)$$

$$\delta\dot{m} = -(\mathrm{i}\widetilde{\Delta}_m + \kappa_m)\delta m - \mathrm{i}g_{ma}\delta a - \mathrm{i}G_{mb}\left(\delta b + \delta b^\dagger\right), \quad (12)$$

$$\delta\dot{b} = -(\mathrm{i}\omega_b + \kappa_b)\delta b - \mathrm{i}\left(G_{mb}^*\delta m + G_{mb}\delta m^\dagger\right) + \mathrm{i}\left(G_{bc}^*\delta c + G_{bc}\delta c^\dagger\right), \quad (13)$$

$$\delta\dot{c} = -(\mathrm{i}\widetilde{\Delta}_c + \kappa_c)\delta c + \mathrm{i}G_{bc}\left(\delta b + \delta b^\dagger\right) + \varepsilon_{\mathrm{p}2}\mathrm{e}^{-\mathrm{i}\delta_2 t}, \quad (14)$$

where $G_{mb} = g_{mb}m_{\mathrm{s}}$ and $G_{bc} = g_{bc}m_{\mathrm{s}}$ are the effective magnomechanical and optomechanical coupling strengths. We linearize the quantum Langevin equation near the steady-state solution and retain only the first-order terms in the fluctuation operators. Each operator can be written as $\delta O = O_+\,\mathrm{e}^{-\mathrm{i}\delta_j t} + O_-\,\mathrm{e}^{\mathrm{i}\delta_j t}$ $(O = a, m, b, c;\ j = 1, 2)$. The magnon and optical cavity modes are driven by the strongly red-detuned microwave and optical fields, respectively,[31] thereby suppressing the highly off-resonant Stokes scattering. As a result, only the anti-Stokes scattering builds up within the cavity.[2,38] In the resolved sideband regime, i.e., $\Delta_a = \widetilde{\Delta}_m = \widetilde{\Delta}_c = \omega_b \gg \kappa_a, \kappa_m, \kappa_c$, the lower sideband and far off-resonance can be safely neglected.[2,39] Therefore, we focus on providing the equations for O_+ as follows:[40]

$$[\mathrm{i}(\Delta_a - \delta_j) + \kappa_a]a_+ = -\mathrm{i}g_{ma}m_+ + \varepsilon_{\mathrm{p}1}, \quad (15)$$

$$\left[\mathrm{i}\left(\widetilde{\Delta}_m - \delta_j\right) + \kappa_m\right]m_+ = -\mathrm{i}g_{ma}a_+ - \mathrm{i}G_{mb}b_+, \quad (16)$$

$$[\mathrm{i}(\omega_b - \delta_j) + \kappa_b]b_+ = -\mathrm{i}G_{mb}^*m_+ + \mathrm{i}G_{bc}^*c_+, \quad (17)$$

$$\left[\mathrm{i}\left(\widetilde{\Delta}_c - \delta_j\right) + \kappa_c\right]c_+ = \mathrm{i}G_{bc}b_+ + \varepsilon_{\mathrm{p}2}. \quad (18)$$

We send a weak probe field with frequency $\omega_{\mathrm{p}1}$ to the microwave cavity, i.e., $j = 1$ and set $\lambda_1 = \omega_b - \delta_1$. The solution for the microwave cavity field is then given by

$$a_+ = \frac{\varepsilon_{\mathrm{p}1}}{\mathrm{i}\lambda_1 + \kappa_a + \dfrac{g_{ma}^2}{\mathrm{i}\lambda_1 + \kappa_m + \dfrac{|G_{mb}|^2}{\mathrm{i}\lambda_1 + \kappa_b + \dfrac{|G_{bc}|^2}{\mathrm{i}\lambda_1 + \kappa_c}}}}. \quad (19)$$

The output field amplitude of the microwave cavity is obtained by the standard input–output relation $\varepsilon_{\mathrm{out}1} = \varepsilon_{\mathrm{in}} - \kappa_a\langle a\rangle$.[36] The amplitude of the output field can therefore be written as

$$\varepsilon_{\mathrm{out}1} = \frac{2\kappa_a a_+}{\varepsilon_{\mathrm{p}1}}. \quad (20)$$

The real $\mathrm{Re}[\varepsilon_{\mathrm{out}}]$ and imaginary $\mathrm{Im}[\varepsilon_{\mathrm{out}}]$ parts of the output field represent the absorption and dispersion spectra of the system. Changing the weak probe field with frequency $\omega_{\mathrm{p}2}$ to the optical cavity, i.e., $j = 2$, we set $\lambda_2 = \omega_b - \delta_2$ and obtain the resulting expression for c_+ as

$$c_+ = \frac{\varepsilon_{\mathrm{p}2}}{\mathrm{i}\lambda_2 + \kappa_c + \dfrac{|G_{bc}|^2}{\mathrm{i}\lambda_2 + \kappa_b + \dfrac{|G_{mb}|^2}{\mathrm{i}\lambda_2 + \kappa_m + \dfrac{g_{ma}^2}{\mathrm{i}\lambda_2 + \kappa_a}}}}. \quad (21)$$

By applying the standard input–output relation, the output field amplitude of the optical cavity can be expressed as

$$\varepsilon_{\mathrm{out}2} = \frac{2\kappa_c c_+}{\varepsilon_{\mathrm{p}2}}. \quad (22)$$

3. Discussion

3.1. The probe field interacts with the microwave cavity

We first study the output spectrum of the cavity-OMM system probed to the microwave cavity. When the frequency of the probe field is tuned to the microwave frequency band, it resonates with the microwave cavity. We use experimentally feasible parameters[10] $\omega_a/2\pi = 10$ GHz, $\omega_m/2\pi = 10$ GHz, $\omega_b/2\pi = 10$ MHz, $\lambda_c = 1550$ nm, $\kappa_a/2\pi = 2.1$ MHz, $\kappa_m/2\pi = \kappa_c/2\pi = 1$ MHz, and $\kappa_b/2\pi = 100$ Hz.

To investigate the effect of the optomechanical effective coupling strength on the output spectrum, we fix the microwave–magnon coupling strength at $g_{ma}/2\pi = 3$ MHz. We systematically investigate the role of various coupling parameters within the system to elucidate the fundamental physics governing multi-band transparency. The fundamental reason for forming transparency windows is the destructive interference between different optical transition paths. To

reveal the mechanism of the MIT, MMIT and OMIT windows more clearly, we plot the energy level diagram of the cavity-OMM system in Fig. 2. Specifically, the state transition $|n_a,n_m,n_b,n_c\rangle \longleftrightarrow |n_a+1,n_m,n_b,n_c\rangle$ is due to the direct excitation of a photon by the probe field. The state transition $|n_a,n_m+1,n_b,n_c\rangle \longleftrightarrow |n_a+1,n_m,n_b,n_c\rangle$ is due to the interaction between the magnon mode and the microwave cavity mode, which annihilates a magnon and creates a photon simultaneously. The two transition paths together lead to destructive interference, resulting in a MIT window at resonance and symmetric absorption dips on both sides. When the phonon mode of the YIG crystal is considered, the magnomechanical interaction introduces the transition path: $|n_a,n_m,n_b+1,n_c\rangle \longleftrightarrow |n_a,n_m+1,n_b,n_c\rangle$, which destroys the original quantum coherence and results in two transparency windows, as shown in Fig. 3(b). Furthermore, the interaction of the optical cavity mode with the phonon mode through radiation pressure induces a phonon conversion process, which can be described as $|n_a,n_m,n_b,n_c+1\rangle \longleftrightarrow |n_a,n_m,n_b+1,n_c\rangle$. The transition path constructively interferes with the aforementioned paths, generating an OMIT window at resonance.

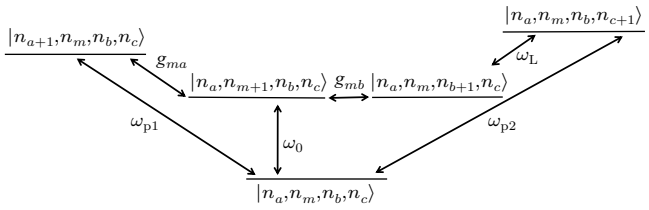


Fig. 2. Schematic of the energy-level diagram of the cavity-OMM system.

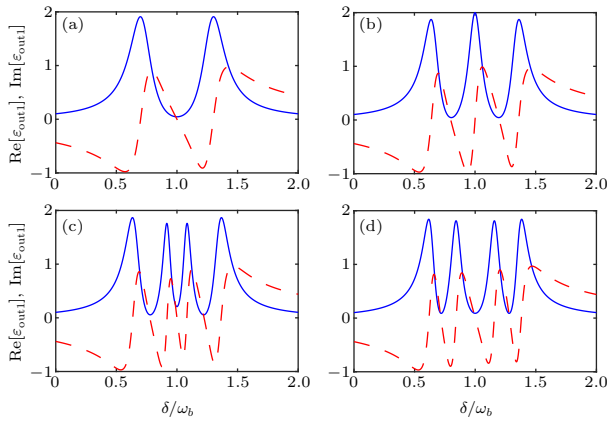


Fig. 3. The absorption profiles (blue line) and dispersion profiles (red dashed line) of the output probe field as a function of the probe detuning δ/ω_b: (a) $G_{mb} = G_{bc} = 0$, (b) $G_{mb}/2\pi = 2$ MHz, $G_{bc} = 0$, (c) $G_{mb}/2\pi$ =2MHz, $G_{bc}/2\pi = 1$ MHz, (d) $G_{mb}/2\pi = G_{bc}/2\pi = 2$ MHz.

Figure 3 presents the spectral response of the probe field in terms of both the absorption and dispersion characteristics of the output field under different coupling strengths. In Fig. 3(a), we assume that only microwave–magnon interaction is present, i.e., $G_{mb} = G_{bc} = 0$. We observe a MIT window in which a typical Lorentzian peak of the simple cavity output spectrum splits into two peaks with a single dip angle at the resonance $\delta = \omega_b$. Then, the introduction of magnomechanical coupling leads to a new transition path, which interferes with the original two paths. The interference creates a new point of destructive interference, which corresponds to the MMIT window, as shown in Fig. 3(b). Therefore, figure 3(b) illustrates the fundamental transparency characteristics of the CMM system in the absence of optomechanical coupling. In this case, the transparency windows are mainly composed of MIT and MMIT, and the probe field is completely absorbed at the resonant frequency.

After the introduction of effective optomechanical coupling, a third OMIT window appears, as shown in Figs. 3(c) and 3(d). The mechanism of this phenomenon is attributed to the transition path introduced by the interaction between the phonon mode and the optical cavity mode via the radiation pressure. Note that as the optomechanical coupling strength G_{bc} increases, the transparency dip (i.e., the dip depth) of the OMIT window deepens. This phenomenon occurs because the enhanced optomechanical interaction improves the energy exchange efficiency between the optical cavity and the phonon. Thus, the quantum interference effect induced by the additional transition path more effectively suppresses the absorption of the probe field at the central frequency. The suppression significantly increases the depth of the transparency window. Moreover, the width of the OMIT window is determined by $(\kappa_b/2) + (G_{bc}/\kappa_c)$,[41,42] so an increase in the coupling strength leads to a broadening of the transparency window's width. Thus, the change in the mode of action leads to the number of transparency windows, and the variation of the coupling strength further affects their width and depth. At the same time, this phenomenon reveals the potential application value of optomechanical coupling in achieving controllable photonic transmission.

Meanwhile, with the appearance of a transparency window in the absorption spectrum, significant dispersion occurs at the symmetric positions around $\delta/\omega_b = 1$, and the corresponding dispersion curves become steeper. This property is significant for investigating the propagation mechanism of fast-slow light in our system.

Subsequently, we investigate the physical mechanisms underlying the asymmetric absorption spectra and Fano resonances in the output fields, which arise from the non-resonant quantum interference effect. The absorption spectra of the probe field as a function of δ/ω_b are presented in Fig. 4, showing the asymmetric Fano resonance phenomena generated under different nonresonant conditions. Specifically, figure 4(a) illustrates that the initially symmetric MIT absorption peaks become asymmetric window profiles with detuned $\tilde{\Delta}_m = 0.5\omega_b$. This asymmetry can be interpreted as the superposition effect of multiple Fano resonances. Upon introducing magnomechanical and optomechanical coupling, double and

triple Fano resonances can be observed in Figs. 4(b) and 4(c). These effects arise from the mutual interference between multiple coherent paths provided by the cavity field through the coupling system. Under the resonance condition $\tilde{\Delta}_m = \omega_b$, the Fano resonance disappears, indicating that the resonance case has an inhibitory effect on the Fano resonance, as shown in Fig. 4(d).

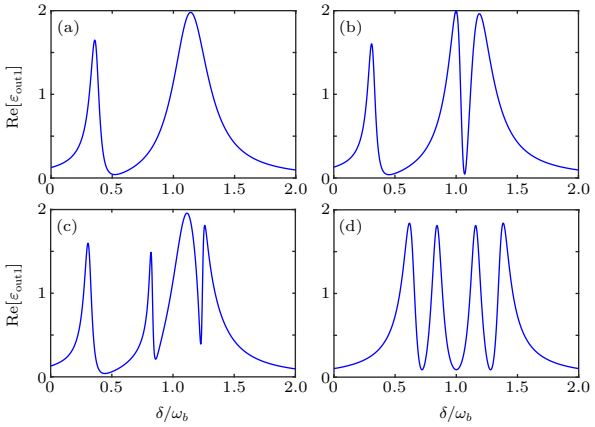


Fig. 4. The Fano lineshapes in the asymmetric real part of the output field $\mathrm{Re}[\varepsilon_{\mathrm{out}}]$ as a function of the probe detuning δ/ω_b: (a) $G_{mb} = G_{bc} = 0$, $\tilde{\Delta}_m = 0.5\omega_b$, (b) $G_{mb}/2\pi = 2$ MHz, $G_{bc} = 0$, $\tilde{\Delta}_m = 0.5\omega_b$, (c) $G_{mb}/2\pi = G_{bc}/2\pi = 2$ MHz, $\tilde{\Delta}_m = 0.5\omega_b$, (d) $G_{mb}/2\pi = G_{bc}/2\pi = 2$ MHz, $\tilde{\Delta}_m = \omega_b$.

We discuss the impact of varying optomechanical effective coupling strengths on the propagation characteristics of fast and slow light within our system. In the narrow transparency window range, the phase of the probe field changes rapidly, denoted as $\phi_t(\omega_{\mathrm{p}}) = \arg[t_{\mathrm{p}}(\omega_{\mathrm{p}})]$. When the phase of the output field undergoes fast oscillation, the group delay can be expressed as[43]

$$\tau = \frac{\partial \phi_t(\omega_{\mathrm{p}})}{\partial \omega_{\mathrm{p}}}. \tag{23}$$

Physically, the positive (negative) value of group delay represents the occurrence of slow (fast) light transmission. Figure 5 plots the group delay τ of the probe field as a function of the normalized probe frequency δ/ω_b at the magnomechanical coupling strength $G_{mb}/2\pi = 2$ MHz.

Figure 5(a) shows the group delay $\tau > 0$ at $\delta = \omega_b$, which corresponds to slow light propagation. With the increase of the optomechanical coupling strength, the propagation characteristic at $\delta/\omega_b = 1$ switches from slow to fast light. The peak value of the group delay on both sides of the resonance frequency changes. Specifically, the positive value increases while the negative value decreases, which indicates that the slow light effect is enhanced and the fast light effect is weakened. This change arises as a result of the optomechanical coupling introducing an additional quantum interference pathway, which induces fast phase dispersion on both sides of the resonance frequency. In short, the physical mechanism of group delay involves tunable quantum interference between the probe field and the anti-Stokes field. Therefore, dynamic control of the group time delay can be achieved by adjusting the strength of the optomechanical coupling, which enables effective modulation of the fast and slow light effects.

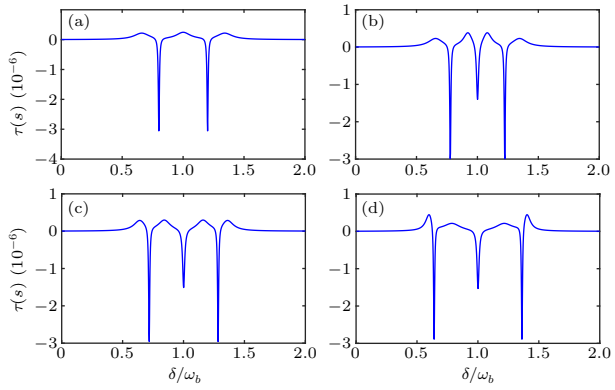


Fig. 5. The group delay of the output field as a function of the probe detuning δ/ω_b for different values of optomechanical effective coupling strength G_{bc}: (a) $G_{bc} = 0$, (b) $G_{bc}/2\pi = 1$ MHz, (c) $G_{bc}/2\pi = 2$ MHz, (d) $G_{bc}/2\pi = 3$ MHz.

3.2. The probe field interacts with the optical cavity

In the following section, we study the output spectrum of the probe field with frequency ω_{p2} acting on the optical cavity. When the frequency of the probe field is tuned to the optical frequency band, it resonates with the optical cavity. To investigate the effect of the microwave cavity on the output spectrum, we assume an optomechanical effective coupling strength $G_{bc}/2\pi = 2$ MHz. Our analysis methodology parallels the approach used in studying the output spectrum of the microwave cavity, employing absorption spectra, dispersion characteristics, Fano resonance profiles, and group delay measurements to investigate system properties.

We explain the physical mechanism of the MIT, MMIT and OMIT phenomena by combining the system energy level transition diagram, as shown in Fig. 6. When $g_{ma} = G_{mb} = 0$, the photon in the system can be generated through two paths: one transition process $|n_a, n_m, n_b, n_c + 1\rangle \longleftrightarrow |n_a, n_m, n_b + 1, n_c\rangle$ achieved via the coupling between the phonon mode and the optical cavity mode under the drive of the laser with frequency ω_{L}; the other one is the direct excitation of the transition path $|n_a, n_m, n_b, n_c\rangle \longleftrightarrow |n_a, n_m, n_b, n_c + 1\rangle$ induced by the probe field. The two different interference paths lead to destructive quantum interference at resonance, resulting in an OMIT window within the originally absorbing frequency band, as shown in Fig. 6(a). Introducing magnomechanical interaction adds a new transition channel $|n_a, n_m, n_b + 1, n_c\rangle \longleftrightarrow |n_a, n_m + 1, n_b, n_c\rangle$, which describes the annihilation of a phonon, the absorption of a driving photon, and the simultaneous creation of a magnon. This transition disrupts the previous quantum coherence, forming two transparency windows, as shown in Fig. 6(b). An additional quantum interference path emerges when the magnon

mode pairs with the microwave cavity mode via magnetic dipole interactions, which leads to the MIT, MMIT and OMT windows observed in Figs. 6(c) and 6(d). Consequently, adjusting the coupling strengths under different interaction modes substantially modifies the conditions for quantum interference. These findings are consistent with the observations presented in Fig. 3.

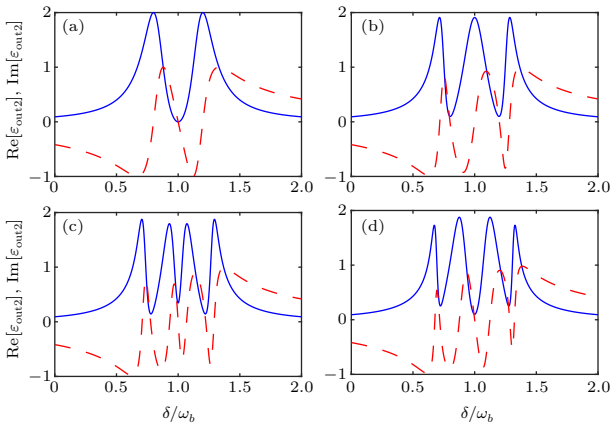


Fig. 6. The absorption profiles (blue line) and dispersion profiles (red dashed line) of the output probe field as a function of the probe detuning δ/ω_b: (a) $g_{ma} = G_{mb} = 0$, (b) $g_{ma} = 0$, $G_{mb}/2\pi = 2$ MHz, (c) $g_{ma}/2\pi = 1$ MHz, $G_{mb}/2\pi = 2$ MHz, (d) $g_{ma}/2\pi = G_{mb}/2\pi = 2$ MHz.

Similarly, the dispersion spectrum shows that the dispersion curve becomes steeper as the transparency window appears on the absorption spectrum. Moreover, the transparency window widens as the effective microwave–magnon coupling is enhanced. Thus, modulating the coupling coefficients realizes the modulation of transparent properties.

Figure 7 explores the influence of coupling parameters on the Fano resonance. Figures 7(a) and 7(c) show the increase in the asymmetric transparency window within the triple Fano resonance spectrum as the coupling coefficient is introduced. This asymmetry is due to the interaction of the nonresonant terms with $\tilde{\Delta}_c = 0.7\omega_b$. With all couplings present, the resonance condition $\tilde{\Delta}_c = \omega_b$ is satisfied. This causes the Fano resonance to disappear and leads to the appearance of a symmetric transparency window in the absorption spectrum, as illustrated in Fig. 7(d). This result demonstrates that the system is in resonance, and the interaction between the different coupled modes reaches an equilibrium that suppresses the Fano resonance.

Next, we illustrate the probe field group delay τ as a function of the normalized frequency δ/ω_b for different microwave–magnon coupling strengths in Fig. 8. We consider the magnomechanical coupling strength $G_{mb}/2\pi = 2$ MHz. The group delay changes significantly with the enhancement of the microwave–magnon interaction. Meanwhile, the fast light at the resonance frequency $\delta = \omega_b$ is increasing and reaches a speed of 5 μs, as shown in Fig. 8(d). In addition, the increasing negative and decreasing positive values on both sides of the resonance frequency indicate that the transition from slow to fast light is achieved.

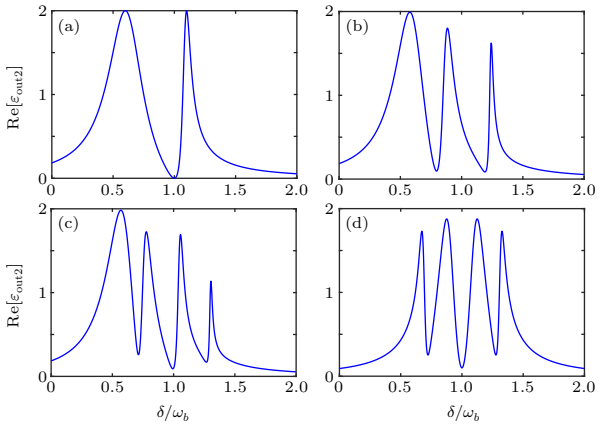


Fig. 7. The Fano lineshapes in the asymmetric real part of the output field $\mathrm{Re}[\varepsilon_{out}]$ as a function of the probe detuning δ/ω_b: (a) $g_{ma} = G_{mb} = 0$, $\tilde{\Delta}_c = 0.7\omega_b$, (b) $g_{ma} = 0$, $G_{mb}/2\pi = 2$ MHz, $\tilde{\Delta}_c = 0.7\omega_b$, (c) $g_{ma}/2\pi = G_{mb}/2\pi = 2$ MHz, $\tilde{\Delta}_c = 0.7\omega_b$, (d) $g_{ma}/2\pi = G_{mb}/2\pi = 2$ MHz, $\tilde{\Delta}_c = \omega_b$.

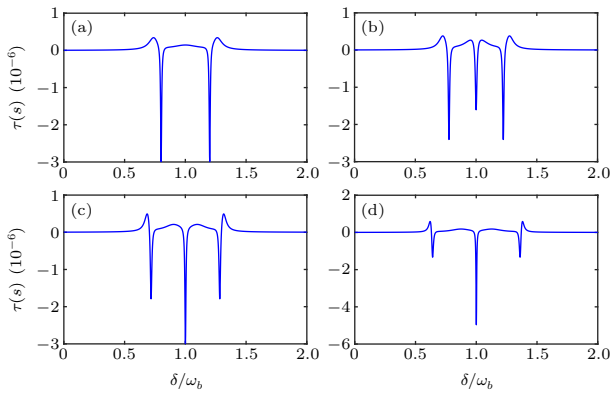


Fig. 8. The group delay of the output field as a function of the probe detuning δ/ω_b for different values of microwave–magnon coupling strength g_{ma}: (a) $g_{ma} = 0$, (b) $g_{ma}/2\pi = 1$ MHz, (c) $g_{ma}/2\pi = 2$ MHz, (d) $g_{ma}/2\pi = 3$ MHz.

Finally, we analyze the experimental feasibility of the proposed model. Current experimental research provides robust support for the physical mechanisms of our system from multiple perspectives. Firstly, existing experiments have confirmed that the MMIT phenomenon in the CMM system can be attributed to the quantum sideband interference effect caused by the coupling between the magnon mode and the phonon mode.[44] Secondly, the collective magnon excitations of the YIG crystal within the microwave cavity can achieve coupling with microwave photons via magnetic dipole interactions,[32] while simultaneously establishing a coupling channel between the magnon and phonon through the magnetostrictive effect.[44] The optical cavity required for optomechanical coupling can be realized by installing a small and highly-reflective mirror pad on the surface of a micro bridge.[45] Furthermore, optomechanical coupling through radiation pressure has been successfully demonstrated in the COM system, achieving OMIT.[2] On this basis, the state-swap interaction among the magnon, phonon and photon is

activated.[17] Therefore, these research findings suggest that the scheme proposed in this study may be experimentally realized.

4. Conclusion

Our study explores the MIT, MMIT and OMIT windows in the cavity-OMM system under weak control fields. By dynamically tuning the probe field frequency to the resonance frequencies of both microwave and optical cavities, we analyze the absorption and dispersion spectra of the output field. This reveals that adjusting the coupling mechanisms and strengths can directly modulate the properties of the transparency window. When the probe field interacts with the microwave cavity, its absorption at the resonance frequency is significantly suppressed under optomechanical coupling. This leads to a pronounced switching effect on light transmission. Additionally, we analyzed the phenomenon of asymmetric Fano resonance, which reflects the presence of quantum interference mechanisms within the system and impacts the processes of fast and slow light conversion. Furthermore, selecting appropriate coupling parameters not only enhances the effects of fast and slow light but also enables dynamic switching between these effects. The study highlights the intricate dynamic behavior of the system, demonstrating that the interaction between microwave and optical fields involves complex quantum interference processes rather than simple superposition. Our work may find applications in research on multiband quantum storage and multi-channel photonic information processing devices.

Acknowledgments

Project supported by the National Natural Science Foundation of China (Grant Nos. 62071376, 62405041, 52175531, and 62005211), the National Key Laboratory of Science and Technology on Space Microwave (Grant No. HTKJ2024KL504002), and the Program of State Key Laboratory of Quantum Optics and Quantum Optics Devices (Grant No. KF202408), and the Natural Science Foundation of Chongqing (Grant No. CSTB2024NSCQ-MSX0746).

References

[1] Kippenberg T J and Vahala K J 2008 *Science* **321** 1172
[2] Weis S, Rivière R, Deléglise S, Gavartin E, Arcizet O, Schliesser A and Kippenberg T J 2010 *Science* **330** 1520
[3] Qin G Q, Yang H, Mao X, Wen J W, Wang M, Ruan D and Long G L 2020 *Opt. Express* **28** 580
[4] Wang B, Nori F and Xiang Z L 2024 *Phys. Rev. Lett.* **132** 053601
[5] Ren Y L, Ma S L, Xie J K, Li X K and Li F L 2021 *Opt. Express* **29** 41399
[6] Zhou B Y and Li G X 2016 *Phys. Rev. A* **94** 033809
[7] Lvovsky A I, Sanders B C and Tittel W 2009 *Nat. Photon.* **3** 706
[8] He Y 2016 *Phys. Rev. A* **94** 063804
[9] Wang Q, Zhang J Q, Ma P C, Yao C M and Feng M 2015 *Phys. Rev. A* **91** 063827
[10] Zuo X, Fan Z Y, Qian H, Ding M S, Tan H, Xiong H and Li J 2024 *New. J. Phys.* **26** 031201
[11] Mihalceanu L, Vasyuchka V I, Bozhko D A, Langner T, Nechiporuk A Y, Romanyuk V F, Hillebrands B and Serga A A 2018 *Phys. Rev. B* **97** 214405
[12] Ullah K, Naseem M T and Müstecaplıoğlu Ö E 2020 *Phys. Rev. A* **102** 033721
[13] Barbhuiya S A and Bhattacherjee A B 2022 *J. Appl. Phys.* **132**
[14] Yang Z, Zhao C, Peng R, Yang J and Zhou L 2023 *Opt. Lett.* **48** 375
[15] Shen R C, Li J, Fan Z Y, Wang Y P and You J Q 2022 *Phys. Rev. Lett.* **129** 123601
[16] Zhang H Q, Chu S S, Zhang J S, Zhong W X and Cheng G L 2024 *Opt. Lett.* **49** 2009
[17] Li J, Zhu S Y and Agarwal G S 2018 *Phys. Rev. Lett.* **121** 203601
[18] Kong D, Xu J, Gong C, Wang F and Hu X 2022 *Opt. Express* **30** 34998
[19] Bayati S, Bagheri Harouni M and Mahdifar A 2024 *Opt. Express* **32** 14914
[20] Agarwal G S and Huang S 2010 *Phys. Rev. A* **81** 041803
[21] Fan Z Y, Qian H, Zuo X and Li J 2023 *Phys. Rev. A* **108** 023501
[22] Chabar N and Amazioug M 2024 *Chin. Phys. B* **33** 120308
[23] Liao Q, Peng K and Qiu H 2023 *Chin. Phy. B* **32** 054205
[24] Engelhardt F, Bittencourt V A S V, Huebl H and Kusminskiy S V 2022 *Phys. Rev. Appl.* **18** 044059
[25] Fano U 1961 *Phys. Rev.* **124** 1866
[26] Lu T X, Xiao X, Chen L S, Zhang Q and Jing H 2023 *Phys. Rev. A* **107** 063714
[27] Zangeneh-Nejad F and Fleury R 2019 *Phys. Rev. Lett.* **122** 014301
[28] Akhtar M S and Naweed A 2024 *Opt. Lett.* **49** 5667
[29] Liu Z X, Xiong H and Wu Y 2019 *IEEE Access* **7** 57047
[30] Fan Z Y, Qian H and Li J 2022 *Quantum. Sci. Technol.* **8** 015014
[31] Li J and Gröblacher S 2021 *Quantum. Sci. Technol.* **6** 024005
[32] Zhang X, Zou C L, Jiang L and Tang H X 2014 *Phys. Rev. Lett.* **113** 156401
[33] Qiu W, Cheng X, Chen A, Lan Y and Nie W 2022 *Phys. Rev. A* **105** 063718
[34] Fan Z Y, Qiu L, Gröblacher S and Li J 2023 *Laser. Photon. Rev.* **17** 2200866
[35] Wang Y P, Zhang G Q, Zhang D, Luo X Q, Xiong W, Wang S P, Li T F, Hu C M and You J Q 2016 *Phys. Rev. B* **94** 224410
[36] Kong C, Wang B, Liu Z X, Xiong H and Wu Y 2019 *Opt. Express* **27** 5544
[37] Huang S and Agarwal G S 2011 *Phys. Rev. A* **83** 043826
[38] Wang Y D and Clerk A A 2012 *Phys. Rev. Lett.* **108** 153603
[39] Jiang C, Liu H, Cui Y, Li X, Chen G and Chen B 2013 *Opt. Express* **21** 12165
[40] Sohail A, Zhang Y, Zhang J and Yu C S 2016 *Sci. Rep.* **6** 28830
[41] Agarwal G S and Huang S 2010 *Phys. Rev. A* **81** 041803
[42] Yan X B 2020 *Phys. Rev. A* **101** 043820
[43] Tarhan D, Huang S and Müstecaplıoğlu Ö E 2013 *Phys. Rev. A* **87** 013824
[44] Zhang X, Zou C L, Jiang, L and Tang H X 2016 *Sci. Adv.* **2** e1501286
[45] Gröblacher S, Hammerer K, Vanner M R and Aspelmeyer M 2009 *Nature* **460** 724